
Improved Detection of Regional Melanoma Metastasis Using ^{18}F -6-Fluoro-*N*-[2-(Diethylamino)Ethyl] Pyridine-3-Carboxamide, a Melanin-Specific PET Probe, by Perilesional Administration

Delphine Denoyer¹, Titaina Potdevin¹, Peter Roselt¹, Oliver C. Neels¹, Laura Kirby¹, Ivan Greguric², Andrew Katsifis², Donna S. Dorow¹, and Rodney J. Hicks^{1,3}

¹Centre for Cancer Imaging and Translational Research Laboratory, Peter MacCallum Cancer Centre, East Melbourne, Victoria, Australia; ²Radiopharmaceuticals Research Institute, Australian Nuclear Science and Technology Organisation, Menai, New South Wales, Australia; and ³Department of Medicine, University of Melbourne, Parkville, Victoria, Australia

The efficacy of differing routes of administration of ^{18}F -6-fluoro-*N*-[2-(diethylamino)ethyl] pyridine-3-carboxamide (^{18}F -MEL050), a new benzamide-based PET radiotracer for imaging regional lymph node metastasis in melanoma, was assessed. **Methods:** B16-Black/6 metastatic melanoma cells harboring an mCherry transgene were implanted into the left-upper-foot surface of 49 C57 Black/6 mice as a model of popliteal lymph node (PLN) metastasis. Ultrasound scanning of the left PLN was performed at baseline and in combination with ^{18}F -MEL050 PET on days 5, 9, and 14. Mice were divided into 2 groups to compare the results of tracer administration either subcutaneously at the tumor site (local) or in the lateral tail vein (systemic). After PET on each imaging day, 5 mice per group—including any with evidence of metastasis—were sacrificed for ex vivo validation studies including assessment of retained radioactivity and presence of the mCherry transgene as a surrogate of nodal tumor burden. **Results:** Nine mice were judged as positive for PLN metastasis by ultrasound at day 5, and 8 PLNs were positive on ^{18}F -MEL050 PET, 3 after systemic and 5 after local administration. Ex vivo analysis showed that ultrasound correctly identified 90% of positive PLNs, with 1 false-positive. ^{18}F -MEL050 PET correctly identified 60% of positive PLNs after systemic administration and 100% after local administration with no false-positive results by either route. The average node-to-background ratio for positive PLNs was 6.8 in the systemic-administration group and correlated with disease burden. In the local-administration group, the mean uptake ratio was 48, without clear relation to metastatic burden. Additional sites of metastatic disease were also correctly identified by ^{18}F -MEL050 PET. **Conclusion:** In addition to its potential for systemic staging, perilesional administration of ^{18}F -MEL050 may allow sensitive and specific, noninvasive identification of regional lymph node metastasis in pigmented malignant melanomas.

Key Words: MEL050; benzamide; melanoma imaging; lymphoscintigraphy; small-animal PET; fluoro-nicotinamide analog

J Nucl Med 2011; 52:115–122

DOI: 10.2967/jnumed.110.078154

Standard clinical practice for the initial treatment of cutaneous melanoma involves wide local excision of the primary lesion and assessment of metastatic spread to lymph nodes draining the tumor site, usually by sentinel lymph node biopsy (SLNB) (1,2). The status of these sentinel lymph nodes with respect to micrometastases is an important factor for both prognostic evaluation and treatment planning. Current methods for sentinel node identification include visual detection intraoperatively with pigmented agents such as methylene blue and use of radiocolloids cleared by reticuloendothelial elements of lymph nodes for mapping by lymphoscintigraphy or detection by γ -probes (3,4). However, in some cases replacement of normal reticuloendothelial cells by melanoma cells may lead to false-negative results (5).

Additional imaging modalities that may be used for visualization, staging, and assessment of regional nodal status are CT, ultrasound, MRI, and ^{18}F -FDG PET (6,7). Each of these techniques has limitations as diagnostic or prognostic tools for melanoma. For instance, CT, ultrasound, or MRI assessment is dependent on nodal size and architecture. These features can be influenced by many factors, reducing accuracy for identification of nodal metastasis (8). Although ultrasound is probably the most accurate anatomic imaging technique for the detection of nodal metastases, it is limited primarily to superficial nodal stations. ^{18}F -FDG PET can play an important role in the staging of cutaneous melanoma, especially in identifying larger nodal deposits, with the additional advantage of potentially identifying occult distant metastasis. However, ^{18}F -FDG PET lacks sufficient

Received Apr. 13, 2010; revision accepted Jun. 25, 2010.

For correspondence or reprints contact: Rodney Hicks, Departments of Medicine and Radiology, University of Melbourne, Centre for Cancer Imaging, Translational Research Laboratory, Molecular Imaging and Targeted Therapeutic Laboratory, Peter MacCallum Cancer Centre, East Melbourne, Victoria 3002, Australia.

E-mail: Rod.Hicks@petermac.org

COPYRIGHT © 2011 by the Society of Nuclear Medicine, Inc.

sensitivity to highlight micrometastasis in regional nodes, particularly when tumor volume is small (9–11). Furthermore, ^{18}F -FDG lacks specificity to discriminate between malignancy and inflammatory lymphadenopathy. Thus, ^{18}F -FDG PET cannot substitute for lymphoscintigraphy and SLNB in melanoma patients (9,12,13). In addition, all of the current imaging modalities for regional staging still require biopsy or excision of the node for histologic confirmation of metastasis (3,14), which can delay definitive management planning and increase the costs of the diagnostic process.

Recently, we reported the synthesis of ^{18}F -6-fluoro-*N*-[2-(diethylamino)ethyl] pyridine-3-carboxamide (^{18}F -MEL050), a new melanoma PET probe with high specificity and avidity for melanin (15). We assessed the imaging potential of ^{18}F -MEL050 using small-animal PET in the B16 model of murine malignant melanoma (16). This study confirmed that ^{18}F -MEL050 has excellent retention in melanin-containing tumors, with rapid clearance from background tissues through urinary excretion. These features afforded high-contrast images, with tumor-to-background ratios of greater than 50:1 at 2 h after tracer injection. Intense uptake was also observed in lung lesions of metastatic melanoma-bearing mice, with a strong concordance between degree of ^{18}F -MEL050 accumulation and tumor burden in the lungs. This high uptake of ^{18}F -MEL050 in small tumor deposits led us to hypothesize that despite partial-volume effects, the avidity of this tracer might be sufficient to detect small-volume regional nodal disease. Moreover, if delivered by draining lymphatic vessels after perilesional administration at the tumor site, analogous to methods used with radiocolloids, ^{18}F -MEL050 might allow visualization of lesions below the theoretic spatial resolution of PET. To test this hypothesis, we used a murine model of lymph node metastasis to evaluate the ability of ^{18}F -MEL050 PET to identify regional lymph node metastases with tracer administered either locally into subcutaneous tissues around the primary tumor site or intravenously. ^{18}F -MEL050 PET was compared with structural imaging with high-resolution small-animal ultrasound. The reference standard for nodal involvement was a combination of visual inspection, *ex vivo* well counting of retained radioactivity, and quantitative real-time polymerase chain reaction (PCR) of an exogenous gene transduced into the tumor cells.

MATERIALS AND METHODS

Cell Lines and Retroviral Transduction

B16-Black/6 (BL/6) cells were maintained in Dulbecco's modified Eagle's medium, 10% fetal calf serum, 2 mM L-glutamine, 1 mM pyruvate, 100 units of penicillin per milliliter, and 100 μg of streptomycin per milliliter. Murine stem cell virus (MSCV)-mCherry-B16-BL/6-clone1 cells were obtained by stable retroviral transduction with an MSCV-mCherry vector (Dr. Patrick Humbert, Peter MacCallum Cancer Centre) derived by replacing the green fluorescent protein (GFP) coding region of MSCV-IRES-GFP (Addgene) with the mCherry coding sequence from pmCherry (Clontech). The MSCV-mCherry vector was transfected into PT67 packaging cells (Clontech) using Lipofectamine (Invi-

trogen) following standard procedures. B16-BL/6 cells were then exposed to filtered MSCV-mCherry-PT67 supernatants containing 8 μg of polybrene per milliliter and MSCV-mCherry-expressing cells enriched by 3 rounds of fluorescence-activated cell sorting (FACSDiva; BD Biosciences) before single-cell clones with the highest mCherry expression were selected by fluorescence-activated cell sorting.

Experimental Model of Lymph Node Metastases

A model of melanoma metastasis to the popliteal lymph node (PLN) was established by injecting 10^6 MSCV-mCherry-B16-BL/6-clone 1 cells in phosphate-buffered saline (25 μL) into the left upper-foot surface of anesthetized (inhalation of 2.5% isoflurane [Abbott Laboratories] in 50% O_2 in air) 10- to 11-wk-old C57BL/6 mice. After 5 d, primary tumors were macroscopically visible at the site of implantation.

Ultrasound Imaging

Volume and morphology of left PLNs was monitored using a Vevo 770 high-resolution small-animal ultrasound system (Visualsonics). For the ultrasound imaging sessions, mice were anesthetized and internal body temperature and respiration continuously monitored using a THM150 physiologic monitoring system (Indus Instruments). Images were acquired in 50- μm increments across the area of the left PLN with a 40-MHz single-element mechanical transducer (focal length, 6 mm; axial resolution, 40 μm ; lateral resolution, 80 μm) mounted perpendicular to the ultrasound beam axis. A 3-dimensional region of interest (ROI) was manually drawn around the PLN on the ultrasound image, and volume was calculated by the standard integrated Vevo 770 software.

^{18}F -MEL050 PET

^{18}F -MEL050 was labeled in an in-house radiochemistry facility, as previously described (15). Briefly, ^{18}F -MEL050 was prepared from 6-chloro-*N*-[2-(diethylamino)ethyl] pyridine-3-carboxamide precursor by a 1-step radiosynthesis using no-carrier-added ^{18}F -KF-Kryptofix 222 (dimethylformamide, 150°C, 5 min), followed by high-performance liquid chromatography purification. Mice were injected either with 20–25 MBq of ^{18}F -MEL050 in 100 μL of saline via the lateral tail vein (systemic) or with 1–1.5 MBq of ^{18}F -MEL050 in 25 μL of saline subcutaneously at the site of the primary tumor (local). Two hours after tracer injection, animals were anesthetized and scanned for 10 min on a Mosaic small-animal PET scanner (Philips; resolution, 2.7 mm at the center of the field of view (17)). An energy window of 450–700 keV and a 6-ns coincidence-timing window were used. Data were acquired in 3-dimensional mode and corrected for isotope decay and random disintegrations. Images were reconstructed with the 3-dimensional row-action maximum likelihood algorithm, and tracer uptake was measured using the ROI software on the Mosaic workstation. Briefly, ROIs were drawn around PLNs and background regions chosen to represent the mediastinal blood pool, excluding regions of tracer accumulation such as the kidneys and spleen. Node-to-background ^{18}F -MEL050 uptake ratios were calculated by dividing the maximum pixel intensity within the node ROI by the average pixel intensity within the background ROI.

Experimental Design

Tumors were implanted into the upper-foot skin of 49 mice in 2 separate experiments. Animals were divided into 2 groups to compare the effect of different routes of tracer administration on PET detection of lymph node metastasis. The size and morphol-

ogy of left PLNs determined by ultrasound before tumor implantation provided a baseline reference for each individual mouse. At day 5, when all animals had small and sometimes diffuse lesions on the foot surface, left PLNs were rescanned by ultrasound, and mice underwent ^{18}F -MEL050 PET. After the PET scan, 5 mice from each group (including any with evidence of metastatic spread by ultrasound or PET) were sacrificed for necropsy and recovery of both popliteal nodes, where possible. At days 9 and 14, ultrasound and PET were repeated for the remaining mice, and 5 animals per group were sacrificed after the scan on each imaging day. At necropsy, mice were examined visually for any signs of melanin-pigmented cells in lymph nodes or other tissues. Excised nodal tissue was weighed, ^{18}F radioactivity measured by well counting, and genomic DNA extracted for PCR assay of the mCherry transgene.

Well Counting and PCR Determination of Nodal Tumor Burden

After PET scans on days 5, 9, and 14, animals were sacrificed, and both PLNs as well as other involved tissues were removed, weighed, and snap-frozen before analysis of retained radioactivity. PLNs were also recovered from 5 naïve mice as controls for PCR analysis of tumor burden. Disintegrations at $511\text{ keV} \pm 15\%$ were quantified in a well counter (187-950-A100 MCA; Biomedex Medical Systems) attached to a multichannel analyzer interfaced with Atomlabs 950 software. After tissues were homogenized in 100 mM NaCl, 10 mM Tris HCl (pH 8), 25 mM ethylenediaminetetraacetic acid, 0.5% sodium dodecyl sulfate, and 0.1 mg of proteinase K per milliliter, genomic DNA was isolated by NaCl extraction and ethanol precipitation (18). A region of the mCherry transgene (supplemental information, available online only at <http://jnm.snmjournals.org>) was amplified by real-time PCR (7900HT Sequence Detection System, version 2.3 software; Applied Biosystems). Relative tumor burden (RTB) was calculated following TaqMan (Applied Biosystems) procedures using the standard formula $(1,000/2^{[Ct\ mCherry - Ct\ vimentin]})$, where Ct (cycle threshold) is the time interval between initiation of amplification and the level of fluorescence passing the threshold set for background amplification. Ct time interval is directly related to the number of copies of the gene of interest in the DNA sample and when corrected for number of cells (vimentin amplification) becomes a surrogate for the number of mCherry-B16-BL/6 melanoma cells in the tissue sample. Data are presented as mean \pm SEM, unless otherwise stated, and Student *t* tests are used for statistical analysis.

RESULTS

Identification of PLN Metastasis by 3-Dimensional Ultrasound

Baseline ultrasound scans showed that all left PLNs were ovoid (normal), with well-delineated regular edges and volumes ranging between 0.29 and 1.31 mm^3 (average, $0.78 \pm 0.03\text{ mm}^3$; $n = 49$). At 5 d after tumor implantation, ultrasound scans revealed that 10 of the 49 mice had an increased left PLN volume, in many cases associated with irregular, crenulated edges suggestive of nodal metastasis (14,19). Typical day 5 ultrasound images for negative and positive PLNs are shown in Figure 1A. Volumes of left PLNs judged to be positive for metastatic changes at day 5 ranged from 2.32 to 19.42 mm^3 (mean, 9.01 ± 0.93

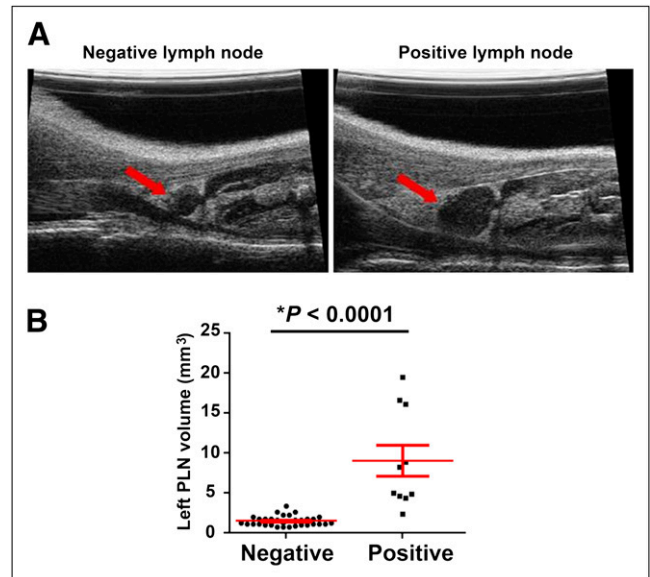


FIGURE 1. Ultrasound examination of PLNs in foot-surface model of melanoma lymph node metastasis. (A) Representative ultrasound images of negative and positive left PLN (arrows) from mice bearing upper-foot-surface B16-BL/6 melanomas at 5 d after tumor implantation. (B) Left PLN volumes calculated from day-5 ultrasound images for mice judged as negative ($n = 39$) or positive ($n = 10$) for left PLN tumor infiltration.

mm^3), whereas nodes judged as negative had volumes between 0.67 and 3.3 mm^3 (mean, $1.47 \pm 0.09\text{ mm}^3$; Fig. 1B). The mean change in volume between baseline and day 5 was $0.68 \pm 0.08\text{ mm}^3$ for negative left PLNs and $8.27 \pm 1.9\text{ mm}^3$ for positive. The ultrasound-calculated volume range for all negative left PLNs from baseline to day 14 was 0.5–4.17 mm^3 , overlapping the positive volumes by approximately 11%. All PLNs judged to be positive were identified at day 5, and no further positive PLNs were detected at days 9 or 14.

^{18}F -MEL050 PET Detection of Lymph Node Metastases

Representative ^{18}F -MEL050 PET images for mice with positive left PLNs in systemic- and local-tracer-administration groups are shown in Figure 2A. Although overall distribution of radioactivity in the mouse body was similar for the 2 routes of administration, tracer uptake in the positive PLNs was considerably enhanced in the local-administration group, compared with the systemic group. This enhanced uptake is exemplified by the clearly superior signal in the PLN of the animal from the local-injection group shown in Figure 2A, despite similar PLN volumes and tissue weights in the 2 mice (systemic: 8.86 mm^3 , 9.12 mg; local: 8.15 mm^3 , 8.28 mg). ^{18}F -MEL050 accumulation in intravenously injected mice was observed in melanin-containing tissues including the eyes, spleen, kidneys, and bladder, indicating mainly urinary elimination, as previously reported (16). However, tracer accumulation in involved nodes and at the tumor site was low with systemic administration. In the local-administration group, the major sites

of accumulation were the injection site and metastatic deposits, including left PLNs (Fig. 2A, arrows), with weaker signals in the eyes, kidneys, and (in some animals) spleen. In both groups, there was a weak signal in the thyroid, as previously reported for ^{18}F -MEL050 (16).

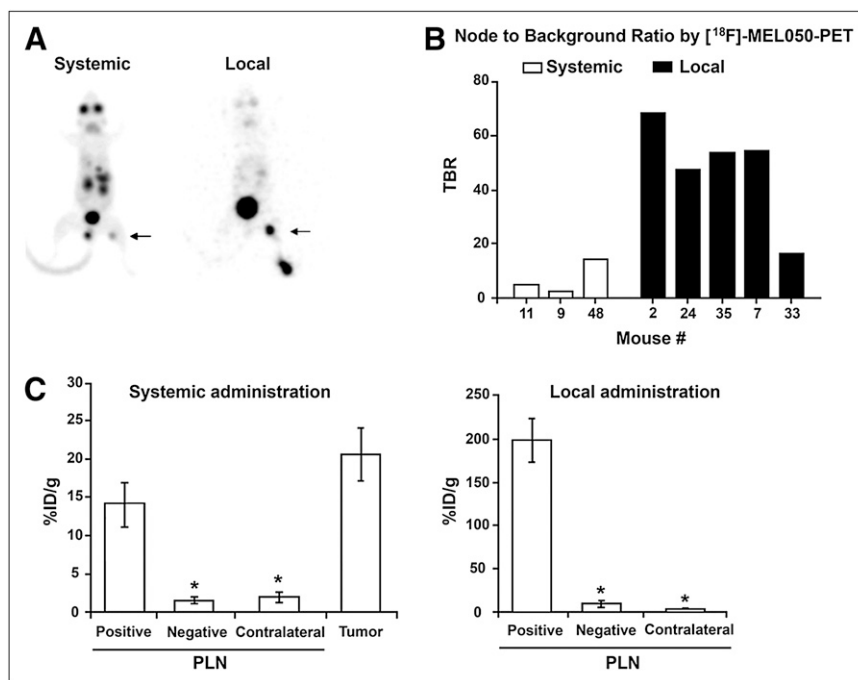
^{18}F -MEL050 accumulation in left PLNs versus background regions (node-to-background ratios), calculated from PET images of animals with PET-positive PLNs, is shown in Figure 2B. Of 24 mice in the systemic group, 3 had positive PLNs on PET, and of the 25 local-injection mice, 5 were judged as positive on the PET scans. The 3 positive PLNs detected by PET in the systemic-injection group had node-to-background ratios of 4.6, 1.9, and 14.0. For the local-injection group, 4 of the 5 positive PLNs had uptake ratios between 47 and 68, whereas that of the fifth and smallest node was 16. On examination of the day-5 PET scans, 1 mouse in the systemic-administration group appeared to have metastatic deposits in the lungs without any sign of metastasis to the PLN. At the day-9 scan, a further 3 mice in this group and 4 in the local-injection group also had evidence of lung metastases on PET without node involvement. The presence of melanin-containing cells in the lungs of each of these mice was confirmed visually at sacrifice. In addition to the lung metastases, on the day-14 PET scan a signal was detected in the subiliac node of a single mouse from the systemic-administration group without evidence of other metastatic lesions (later confirmed *ex vivo* as metastatic involvement of the subiliac node). The subiliac node resides in the mouse flank near the deep circumflex iliac artery (20).

Immediately after PET, mice were sacrificed for thorough necropsy. Both left and right PLNs were recovered where possible, and on the final scanning day the foot-

surface tumors were also recovered from 5 systemic-administration mice. In the case of negative PLNs, some nodes could not be recovered because of difficulty in identifying nodal tissue. For contralateral nodes that were generally small, nodes from 3 to 5 animals were pooled to yield sufficient tissue for weighing and radioactivity measurements. The mean weight of positive left PLNs was 6.72 ± 1.78 mg ($n = 10$), and negative PLNs were 1.61 ± 0.19 mg ($n = 31$). The average weight of contralateral PLNs was 0.55 ± 0.08 mg. Two of the mice in the systemic group that were negative by PET (mice 14 and 18) had evidence of melanin-containing cells in left PLNs at necropsy and were thus considered positive for left PLN metastasis. One of these mice had signs of metastatic changes in the left PLN on ultrasound, but a signal above background could not be detected by PET; for the other, however, involvement of the left PLN was not detected by either ultrasound or PET.

Retained ^{18}F radioactivity measurements (Fig. 2C) confirmed that ^{18}F -MEL050 uptake in PLNs was significantly higher with local tracer injection than with systemic administration. Mean percentage injected dose per gram (%ID/g) for positive PLNs was 14.2 ± 2.9 in the systemic group versus 197.6 ± 24.4 in the local-injection group ($n = 5$ /group). Mean %ID/g for negative left PLNs was also higher in the local-injection group (8.5 ± 1.7 , $n = 16$) than in the systemic group (1.7 ± 0.3 , $n = 15$). However, on the PET images there was no detectable signal for any PLN judged as negative by reference methods, and there were no false-positives on PET. For contralateral PLNs, the %ID/g was much the same for the 2 routes of administration (2 ± 0.6 for systemic and 2.7 ± 0.7 for local, based on 5 pools each containing 3–5 right PLNs). In the systemic group, retained

FIGURE 2. Assessment of draining lymph node metastases in foot-surface tumor-bearing mice. (A) Representative whole-body ^{18}F -MEL050 PET images of upper-foot-surface B16-BL/6 tumor-bearing mice at 2 h after either intravenous injection of 20 MBq of ^{18}F -MEL050 (systemic administration) or subcutaneous perilesional injection of 1 MBq of ^{18}F -MEL050 at primary tumor site (local administration). Arrows indicate left PLNs. (B) Node-to-background ratios determined from PET scans for positive PLNs in systemic- or local-injection groups for each individual mouse indicated by their experimental number (mouse #). (C) Mean %ID/g measured by well counting of tissues at necropsy for PLN and tumor tissues as indicated in systemic or local injection groups. In the case of contralateral PLNs, nodes of 3–5 mice were pooled before weighing and well counting. Results are shown as mean \pm SEM: $n = 5$ positive PLNs, 15 systemic and 16 local negative PLNs, and 5 pools of 3–5 contralateral PLNs each. * $P < 0.05$.



radioactivity in foot-surface tumors was only slightly higher than that in positive PLNs (20.6 ± 3.3 , $n = 5$).

Validation of Metastatic Burden in PLNs by PCR Amplification of mCherry Transgene

In Figure 3A, photographs of 3 positive PLNs with different levels of metastatic infiltration, 1 negative PLN, and 1 PLN from a naïve mouse are shown above a graph of corresponding PCR-based tumor burdens (RTBs). This analysis illustrates the correlation between the degree of infiltration of tumor cells in the node and the number of copies of the mCherry transgene in genomic DNA isolated from nodal tissue. In Figure 3B, RTBs for positive PLNs in both systemic- and local-tracer-administration animals are graphed together with retained activity of ^{18}F -MEL050 from well counting. These data show clearly the superior tracer uptake in relation to tumor burden for local, compared with systemic, administration and confirm the overall concordance of real-time PCR results with ^{18}F -MEL050 uptake, especially in the systemic group.

Results of PET and validation studies for the 2 tracer-administration groups are summarized in Figure 4A. When ^{18}F -MEL050 PET node-to-background and ex vivo well counting assessments are compared with the extent of infiltration of melanoma cells into positive PLNs, it is clear that results generated by PET generally agree with ex vivo anal-

ysis of tracer uptake. Further, it is obvious that uptake of ^{18}F -MEL050 into involved nodes is significantly greater with local than with systemic injection, whether measured by PET or ex vivo well counting. The average ^{18}F -MEL050 PET node-to-background ratio was 6.8 for the systemic-administration group, compared with 48 for the local-injection group. Although the burden of melanoma cells in PLNs in the local-administration group was coincidentally larger than that of the systemic group (mean RTB, $1,011 \pm 273$ for the local group vs. 519 ± 185 for the systemic group), PET detection efficiency is nearly 7-fold higher for local administration, confirming that PET contrast is significantly higher in this group. This result is supported by the ex vivo measurements for retained radioactivity per gram of nodal tissue, which show a 14-fold higher retention of ^{18}F -MEL050 in positive PLNs in the local group. In addition, there was a strong association between intensity of uptake measured by well counting and tumor burden assessed by quantitative PCR (Fig. 4B) in the systemic group, with an R^2 of 0.9764. This strong relationship was not seen after local administration ($R^2 = 0.1635$).

DISCUSSION

To investigate the potential of ^{18}F -MEL050 PET for clinical detection of lymph node metastasis, murine metastatic

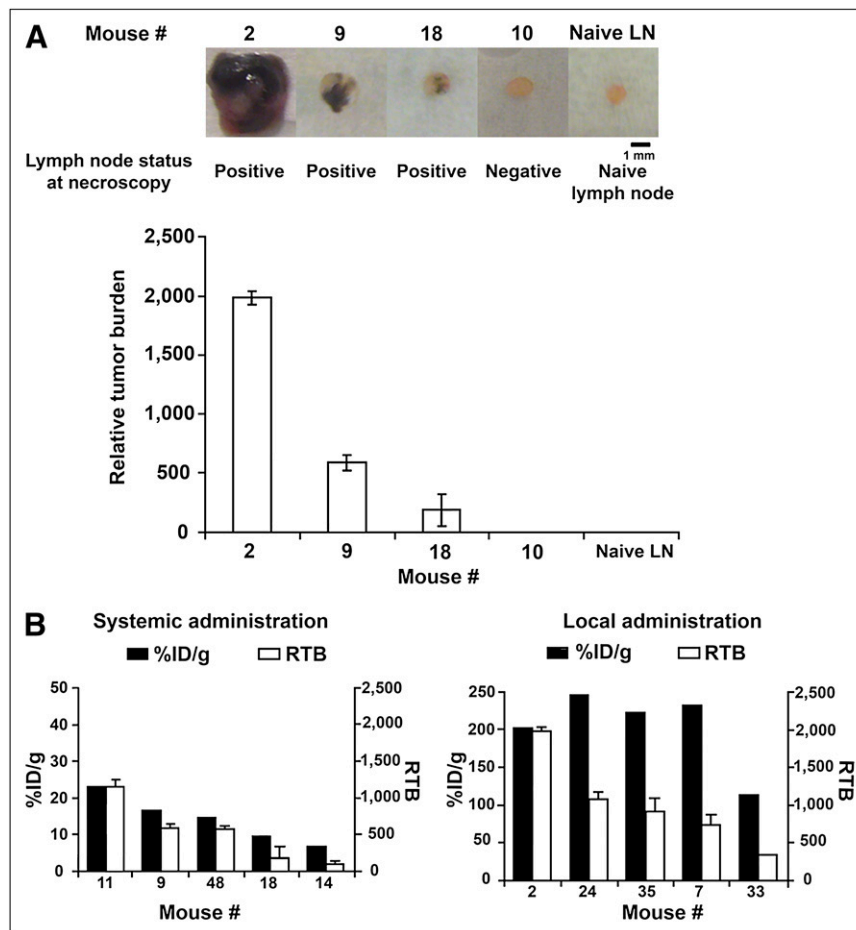


FIGURE 3. Metastatic infiltration into PLNs as determined by visual examination, well counting of retained radioactivity, or real-time PCR. (A) Photographs of 3 left PLNs with different levels of tumor infiltration, 1 negative node, and 1 uninvolved node. Corresponding RTBs for same nodes based on real-time PCR amplification of mCherry transgene are shown in graph below. (B) ^{18}F -MEL050 uptake in positive PLNs expressed as %ID/g (black bars) and RTBs for same PLNs (white bars). RTB mean \pm SEM is based on 3 separate real-time PCR experiments per sample, each with triplicate amplifications.

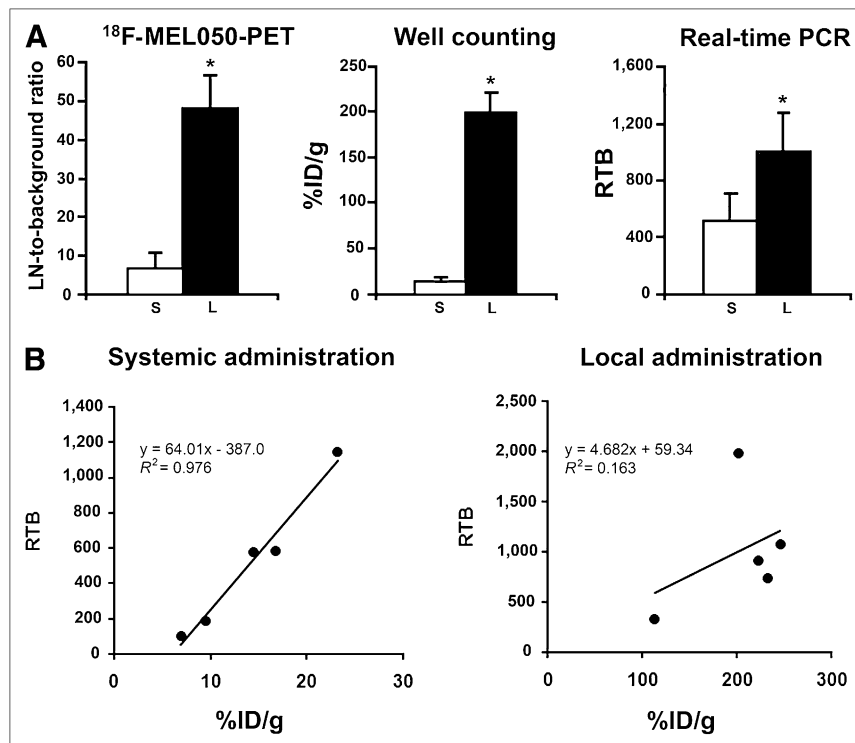


FIGURE 4. Validation of ^{18}F -MEL050 PET as method to determine node infiltration in foot-surface model of metastatic melanoma. (A) Comparison of node-to-background ratios for positive PLNs determined by ^{18}F -MEL050 PET, %ID/g determined by well counting, and RTB from real-time PCR for positive nodes in ^{18}F -MEL050 systemic- (S, white bars) or local- (L, black bars) injection groups. Results are shown as mean \pm SEM (systemic, $n = 3$; local, $n = 5$; well counting and real-time PCR, $n = 5$ per group). (B) Correlation between %ID/g and RTB for systemic- and local-administration groups. * $P < 0.05$.

melanoma B16-BL/6 cells were engineered to express the mCherry gene (21) as a quantifiable marker for extent of PLN metastasis. We used upper-foot dermal implantation rather than foot-pad implantation for several reasons. First, we believed that foot-surface lesions would more closely mimic cutaneous melanoma and therefore offer a realistic model of this disease. Second, lymphatic drainage of the upper surface of the hind foot is likely to favor the PLN—the first-echelon node draining the foot area in the mouse and thus acting as the sentinel node. This location also allowed the use of ultrasound detection of changes in the draining PLN to assist with identification of metastasis-positive nodes. A further consideration was that foot-pad tumors have ethical implications for animal studies because they impede free movement of the mice. Overall, 20% of tumors metastasized to the left PLN, whereas 16% metastasized to the lungs, which are the expected site of metastasis when B16-BL/6 cells are implanted intravenously. Not all dermal tumors led to PLN metastasis, and animals that did develop metastatic lesions had variable disease burdens, paralleling the clinical situation in which metastatic burden is highly variable. The presence of lung metastasis without PLN involvement in some animals suggests that some dermal tumors invaded the circulation, again mimicking the clinical environment in which systemic metastasis can exist in the absence of apparent regional nodal involvement. Such findings are also consistent with previous observations using the foot-pad model, for which the incidence of melanoma spread to the PLNs was reported to range between 11% and 90%, whereas

20%–56% of metastases were to the lungs (22). In the current study, the 8 animals for which lung metastases were detected were evenly divided between the 2 tracer-administration groups, suggesting that detection of distant metastases is not precluded by local injection of ^{18}F -MEL050.

One small metastatic lesion in a subiliac node was detected by ^{18}F -MEL050 PET at day 14 and confirmed at necropsy and further by mCherry real-time PCR (data not shown). In this case, the subiliac metastasis occurred without any indication of involvement of the left PLN (the presumed sentinel node) or other metastatic lesions in the animal. Such a scenario is frequently observed in melanoma patients and represents one of the major drawbacks of SLNB for determining the pathologic stage of the lymphatic chain (23), further emphasizing the need for more specific imaging agents that allow for whole-body staging of melanoma metastases together with identification of sentinel node status. It is encouraging that the presence of unexpected metastatic disease was readily detected by ^{18}F -MEL050 PET. This finding confirms the ability of ^{18}F -MEL050 PET to add information about more distant metastasis in the context of sentinel lymph node investigations. Taken together with its strong promise for whole-body staging, these results suggest that ^{18}F -MEL050 has the potential to considerably improve treatment planning for melanoma over the other existing PET tracers.

As in the clinical situation, we demonstrated that although most PLNs with melanoma infiltration had larger ultrasound volumes than those of negative nodes, there was

still more than a 10% overlap in volume ranges between positive and negative nodes. As suggested by various clinical and preclinical studies (14,19), we used architectural criteria on ultrasound images together with changes in nodal volume to predict the presence of metastases in PLNs. Although PLN status was successfully predicted by these methods in 47 of the 49 mice studied, 1 PLN was judged as false-negative and 1 as false-positive by ultrasound. In this context, we had the advantage of defined baseline PLN volume measurements affording accurate information on changes in nodal size during tumor growth. Such information would rarely be available in the clinical situation. Thus, despite high spatial resolution this anatomic imaging modality still has some limitations for the detection of sentinel lymph node status in melanoma, particularly for smaller deposits.

To address the question of how best to use ^{18}F -MEL050 for identification of sentinel lymph node status, we compared results for 2 clinically relevant routes of administration. Thus, tracer was administered either adjacent to the site of the primary lesion, as currently used in clinical practice for sentinel node lymphoscintigraphy in melanoma, or intravenously to allow systemic delivery, as for ^{18}F -FDG PET. In the systemic-administration group, 3 of 5 positive PLNs were detected by ^{18}F -MEL050 PET, with the 2 remaining positive nodes (nodes 14 and 18) identified at necropsy. These 2 nodes had by far the lowest ^{18}F -MEL050 uptake and correspondingly the smallest tumor burdens of all of the positive PLNs in the study (Fig. 3B). Therefore, signals from these nodes after systemic administration were most likely below the spatial resolution of the PET scanner.

In the case of local administration, all 5 PLNs containing metastases were detected by ^{18}F -MEL050 PET, despite the injected dose being about one twentieth of that used for intravenous injection. However, uptake did not appear to strongly relate to tumor burden with local administration, whereas there was a strong relationship after systemic delivery. These observations are consistent with an increased degree of trapping by a high-capacity, unsaturable target, as would be predicted by the strong avidity of ^{18}F -MEL050 for melanin pigment. When injected intravenously, ^{18}F -MEL050 circulates throughout the body, with only that proportion of tracer delivered by arterial blood being trapped in melanin-pigmented tissues. Because of the rapid elimination of this tracer via the kidneys, the concentration in arterial blood decreases quickly, diminishing background activity and leading to high tumor-to-background ratios but potentially limiting bioavailability to metastatic deposits in lymph nodes. Conversely, after subcutaneous injection most of the ^{18}F -MEL050 is likely to traverse the lymphatic system before reaching the blood circulation. Therefore, ^{18}F -MEL050 concentration in the draining lymphatic basin will be higher, yielding enhanced uptake and increased contrast for even small numbers of pigmented cells within lymphatic tissues. Nevertheless,

some tracer clearly enters the bloodstream, as confirmed by visualization of eyes and spleen tissues in images of locally injected mice (Fig. 2A), albeit with lower intensity than observed with systemic administration. Notably, neither in vivo imaging nor ex vivo counting studies showed any evidence of nonspecific trapping of ^{18}F -MEL050 in draining nodes after local administration.

For the local-injection method, all positive PLNs that were defined visually, by well counting or real-time PCR, were clearly detected by ^{18}F -MEL050 PET, with node-to-background averages greater than 47:1 for 4 of 5 animals. These node-to-background averages were in keeping with our previously reported tumor-to-background ratios of greater than 50:1 for melanotic tumor grafts (16). By comparison, a recent report described imaging of nodal melanoma metastases in the murine foot-pad model using ^{18}F -2'-fluoro-2'-deoxy-1- β -D- β -arabinofuranosyl-5-ethyluracil (^{18}F -FEAU) PET after infection of the primary tumor with an oncolytic herpes virus. In that study, a tumor-to-background ratio of less than 3 and a %ID/g below 1 were reported (24). Moreover, the background signal for ^{18}F -FEAU PET is high, especially in the intestines, requiring degutting of the mice before imaging. Added to the necessity for injection of live virus into the tumor and a 2-d wait for viral replication in vivo before imaging, there is some question as to feasibility of translation of ^{18}F -FEAU PET to the clinic.

In a previous clinical study, ^{125}I - and ^{131}I -labeled methylene blue dyes were shown to specifically bind to melanin and successfully identify many melanotic lesions by γ -camera or SPECT (25). These studies used systemic administration of fairly high doses of iodinated dye, and although initially promising for metastatic melanoma imaging, no trial of local administration for regional lymph node detection or further clinical development has been noted. Even if feasible, the more favorable handling and imaging characteristics of ^{18}F suggest that ^{18}F -MEL050 has much greater potential for clinical development.

In the clinical context, a positive regional ^{18}F -MEL050 scan would eliminate the need for SLNB and allow formal lymph node dissection to be planned after excluding wider metastatic disease, possibly by PET with systemic administration of ^{18}F -MEL050. A negative regional ^{18}F -MEL050 scan could still be followed by conventional radiocolloid lymphoscintigraphy, with SLNB to rule out the presence of micrometastasis in sentinel nodes, which may still be below the detection threshold for ^{18}F -MEL050 PET even with perilesional administration. Such an algorithm would reduce unnecessary SLNB for patients with involved nodes, improving the efficiency and timeliness of definitive treatment planning.

CONCLUSION

In addition to its promise for whole-body staging of cutaneous pigmented melanoma, ^{18}F -MEL050 PET has the potential to act as a regional probe to noninvasively identify

lymph node involvement when injected locally at the primary lesion site.

ACKNOWLEDGMENTS

We gratefully acknowledge Susan Jackson, Rachael Walker, Kerry Ardley, and Jeannette Valentan for technical assistance. This study was funded by the Australian Government Cooperative Research Centre for Biomedical Imaging Development Ltd. (CRCBID), Bundoora, Victoria, Australia.

REFERENCES

1. Scott JD, McKinley BP, Bishop A, Trocha SD. Treatment and outcomes of melanoma with a Breslow's depth greater than or equal to one millimeter in a regional teaching hospital. *Am Surg*. 2005;71:198–201.
2. Phan GQ, Messina JL, Sondak VK, Zager JS. Sentinel lymph node biopsy for melanoma: indications and rationale. *Cancer Control*. 2009;16:234–239.
3. Dias Moreira R, Altino de Almeida S, Maliska Guimaraes CM, Resende JF, Gutfilen B, Barbosa da Fonseca LM. Sentinel node identification by scintigraphic methods in cutaneous melanoma. *J Exp Clin Cancer Res*. 2005;24:181–185.
4. Intenzo CM, Truluck CA, Kushen MC, Kim SM, Berger A, Kairys JC. Lymphoscintigraphy in cutaneous melanoma: an updated total body atlas of sentinel node mapping. *Radiographics*. 2009;29:1125–1135.
5. Lam TK, Uren RF, Scolyer RA, Quinn MJ, Shannon KF, Thompson JF. False-negative sentinel node biopsy because of obstruction of lymphatics by metastatic melanoma: the value of ultrasound in conjunction with preoperative lymphoscintigraphy. *Melanoma Res*. 2009;19:94–99.
6. Ho Shon IA, Chung DK, Saw RP, Thompson JF. Imaging in cutaneous melanoma. *Nucl Med Commun*. 2008;29:847–876.
7. Mohr P, Eggermont AM, Hauschild A, Buzaid A. Staging of cutaneous melanoma. *Ann Oncol*. 2009;20(suppl 6):vi14–vi21.
8. Ferrer R. Lymphadenopathy: differential diagnosis and evaluation. *Am Fam Physician*. 1998;58:1313–1320.
9. Singh B, Ezziddin S, Palmedo H, et al. Preoperative ¹⁸F-FDG-PET/CT imaging and sentinel node biopsy in the detection of regional lymph node metastases in malignant melanoma. *Melanoma Res*. 2008;18:346–352.
10. Krug B, Crott R, Lonneux M, Baurain JF, Pirson AS, Vander Borgh T. Role of PET in the initial staging of cutaneous malignant melanoma: systematic review. *Radiology*. 2008;249:836–844.
11. Veit-Haibach P, Vogt FM, Jablonka R, et al. Diagnostic accuracy of contrast-enhanced FDG-PET/CT in primary staging of cutaneous malignant melanoma. *Eur J Nucl Med Mol Imaging*. 2009;36:910–918.
12. Belhocine T, Pierard G, De Labrassinne M, Lahaye T, Rigo P. Staging of regional nodes in AJCC stage I and II melanoma: ¹⁸F-FDG PET imaging versus sentinel node detection. *Oncologist*. 2002;7:271–278.
13. Jimenez-Requena F, Delgado-Bolton RC, Fernandez-Perez C, et al. Meta-analysis of the performance of ¹⁸F-FDG PET in cutaneous melanoma. *Eur J Nucl Med Mol Imaging*. 2010;37:284–300.
14. Sanki A, Uren RF, Moncrieff M, et al. Targeted high-resolution ultrasound is not an effective substitute for sentinel lymph node biopsy in patients with primary cutaneous melanoma. *J Clin Oncol*. 2009;27:5614–5619.
15. Greguric I, Taylor SR, Denoyer D, et al. Discovery of [¹⁸F]N-(2-(diethylamino)ethyl)-6-fluoronicotinamide: a melanoma positron emission tomography imaging radiotracer with high tumor to body contrast ratio and rapid renal clearance. *J Med Chem*. 2009;52:5299–5302.
16. Denoyer D, Greguric I, Roselt P, et al. High-contrast PET of melanoma using ¹⁸F-MEL050, a selective probe for melanin with predominantly renal clearance. *J Nucl Med*. 2010;51:441–447.
17. Huisman MC, Reder S, Weber AW, Ziegler SI, Schwaiger M. Performance evaluation of the Philips MOSAIC small animal PET scanner. *Eur J Nucl Med Mol Imaging*. 2007;34:532–540.
18. Miller SA, Dykes DD, Polesky HF. A simple salting out procedure for extracting DNA from human nucleated cells. *Nucleic Acids Res*. 1988;16:1215.
19. Saiag P, Bernard M, Beauchet A, Bafounta ML, Bourgault-Villada I, Chagnon S. Ultrasonography using simple diagnostic criteria vs palpation for the detection of regional lymph node metastases of melanoma. *Arch Dermatol*. 2005;141:183–189.
20. Van den Broeck W, Derore A, Simoens P. Anatomy and nomenclature of murine lymph nodes: descriptive study and nomenclatory standardization in BALB/cAnNCrI mice. *J Immunol Methods*. 2006;312:12–19.
21. Shaner NC, Campbell RE, Steinbach PA, Giepmans BN, Palmer AE, Tsien RY. Improved monomeric red, orange and yellow fluorescent proteins derived from *Discosoma* sp. red fluorescent protein. *Nat Biotechnol*. 2004;22:1567–1572.
22. Nathanson SD, Anaya P, Avery M, Hetzel FW, Sarantou T, Havstad S. Sentinel lymph node metastasis in experimental melanoma: relationships among primary tumor size, lymphatic vessel diameter and ^{99m}Tc-labeled human serum albumin clearance. *Ann Surg Oncol*. 1997;4:161–168.
23. Chakera AH, Hesse B, Burak Z, et al. EANM-EORTC general recommendations for sentinel node diagnostics in melanoma. *Eur J Nucl Med Mol Imaging*. 2009;36:1713–1742.
24. Brader P, Kelly K, Gang S, et al. Imaging of lymph node micrometastases using an oncolytic herpes virus and [¹⁸F]FEAU PET. *PLoS ONE*. 2009;4:e4789.
25. Link EM, Blower PJ, Costa DC, et al. Early detection of melanoma metastases with radioiodinated methylene blue. *Eur J Nucl Med*. 1998;25:1322–1329.